Published online November 23, 2004

6120–6128 *Nucleic Acids Research, 2004, Vol. 32, No. 20*
doi:10.1093/nar/gkh949

RNA aptamers selected against the receptor activator of NF-κB acquire general affinity to proteins of the tumor necrosis factor receptor family

Tadashi Mori, Akihiro Oguro[1], Takashi Ohtsu[1] and Yoshikazu Nakamura[1,*]

Research and Development Division, Mitsubishi Pharma Corporation, 1000, Kamoshida-cho, Aoba-ku, Yokohama 227-0033, Japan and [1]Department of Basic Medical Sciences, Institute of Medical Science, University of Tokyo, 4-6-1 Shirokanedai, Minato-ku, Tokyo 108-8639, Japan

Received October 12, 2004; Revised and Accepted October 31, 2004

ABSTRACT

The receptor activator of NF-κB (RANK) is a member of the tumor necrosis factor (TNF) receptor family and acts to cause osteoclastgenesis through the interaction with its ligand, RANKL. We isolated RNA aptamers with high affinity to human RANK by SELEX. Sequence and mutational analysis revealed that the selected RNAs form a G-quartet conformation that is crucial for binding to RANK. When the aptamer binding to RANK was challenged by RANKL, there was no competition between the aptamer and RANKL. Instead, the formation of a ternary complex, aptamer–RANK–RANKL, was detected by a spin down assay and by BIAcore surface plasmon resonance analysis. Moreover, the selected aptamer efficiently bound to other TNF receptor family proteins, such as TRAIL-R2, CD30, NGFR as well as osteoprotegerin, a decoy receptor for RANK. These results suggest that the selected aptamer recognizes not the ligand-binding site, but rather a common structure conserved in the TNF receptor family proteins.

INTRODUCTION

The receptor activator of NF-κB (RANK) is a member of the tumor necrosis factor (TNF) receptor family. RANK acts to cause osteoclastgenesis through the interaction with the RANK ligand, RANKL (1). Ligands and receptors of the TNF superfamily function as signal transducers whose integrated actions impinge principally on the development, homeostasis and adaptive responses of the immune system. Despite their varied and pleiotropic actions, members of the TNF ligand and receptor families have remarkably similar structures and a conservative mode of interaction. In fact, several TNF ligand family proteins utilize multiple TNF receptors (2–6). RANK binds to its ligand RANKL and initiates a cascade of signaling events that leads to osteoclast differentiation. Osteoclasts are known to contribute to focal bone erosion in rheumatoid arthritis (RA) (7). Osteoclasts are also implicated in the pathogenesis of various primary and secondary bone malignancies. In animal models, administration of soluble RANK is able to effectively control humoral hypercalcemia during malignancy thereby preventing cancer-induced skeletal pain and bone loss associated with immobilization (8). Therefore, from a therapeutic view of RA and other bone resorption diseases, it is important to find and develop effective inhibitors that block RANK-mediated signal transduction. For this aim, a clinical trial has been initiated with human recombinant osteoprotegerin (OPG), a decoy receptor for RANKL, to evaluate its potential as an inhibitor of osteoclast differentiation (9).

Treatment of patients with genetically engineered antibodies against targets such as CD20, Her2 and TNF-α has the great advantage of specificity. One of the disadvantages of the antibody therapy, however, is that upon therapeutic antibody injection, the immune system starts reacting against these engineered antibodies leading to neutralization. The technique of *in vitro* RNA selection-amplification (referred to as SELEX) has been used to isolate high affinity oligonucleotides (referred to as aptamers) from randomized RNA libraries that recognize a wide range of target molecules with affinities and specificities comparable with those of antibodies (10,11). A comparison of RNA aptamers with the therapeutic antibody reveals several outstanding features. First, RNA aptamers do not trigger an immune response. Second, synthetic aptamers do not generally exhibit batch-to-batch variation and are amenable to diverse, targeted, chemical modifications. Third, SELEX allows the opportunity to determine conditions for fine tuning aptamers to a given application. Fourth, since RNA aptamers are synthesized chemically, the total cost of synthesis may be lower than that of antibody. Therefore, RNA aptamers have the potential to become an important means of therapeutic application in the future.

In this study, we aimed at generating RNA aptamers against human RANK to develop potential therapeutics for RA and bone malignancies. In the literature, only a few RNA aptamers are known to be reactive to membrane proteins including receptors (12,13). Of these, RNA aptamers against hepatocyte growth factor (HGF) receptor (c-met) were successfully generated by SELEX when HGF's soluble extracellular domain was used as the target molecule (12). By a similar strategy, we chose the extracellular domain of RANK as a target molecule for selecting RNA aptamers. Considering that the ligand RANKL protein is slightly acidic, we anticipated that RNA

*To whom correspondence should be addressed. Tel: +81 3 5449 5307; Fax: +81 3 5449 5415; Email: nak@ims.u-tokyo.ac.jp

aptamers might have a possibility to bind to the ligand-binding site of RANK. The selected RNA aptamers were sequenced and examined by site-directed mutagenesis and *in vitro* binding studies. The findings presented here reveal that the selected aptamers recognize not only RANK but also other TNF receptor family proteins, showing conservative site recognition.

MATERIALS AND METHODS

Reagents

Recombinant human soluble RANK/IgG_1Fc chimera was purchased from R&D Systems. The extracellular domain (Gln29-Gly213) of human RANK (14) was fused to the signal peptide of CD33 at its amino-terminus and also fused to His_6-tagged Fc region of human immunoglobulin G1 (IgG1) at its C-terminus via a 7-amino acid-polypeptide linker. The chimeric protein was expressed in a mouse myeloma cell line, NS0. Mouse RANK, OPG, TRAIL-R2, CD30, NGFR and CD28 were purchased from R&D Systems. Protein kinase C (PKC) was purchased from Calbiochem. RANKL was purchased from Pepro Tech.

Selection-amplification of RNAK aptamers

In vitro RNA selection was performed as described previously (15,16) and the selection scheme is summarized in Table 1. Briefly, transcription templates were synthesized by PCR using synthetic oligonucleotides: 5′-TAATACGACTCACTATAGGGACACAATGGACG (40N) TAACGGCCGACATGAGAG-3′, where 40N represents 40 random nucleotide positions. PCR primer sets used are 40N template, 5′-TAATACGACTCACTATAGGGACACAATGGACG-3′ and 5′-CTCTCATGTCGGCCGTTA-3′, where T7 promoter sequence is underlined. 40N RNA pools were prepared by *in vitro* transcription with T7 RNA polymerase (Takara Co.). RNAs were refolded by heat denaturing at 85°C and rapid cooling to 4°C in buffer A (20 mM Tris–HCl, pH 7.6, 80 mM potassium acetate, 2.5 mM magnesium acetate and 1 mM DTT). Selections were performed in buffer A containing 100 U of RNase inhibitor (Takara Co.). In selection I, RANK was mixed with 3 µl of TALON metal affinity resin (Clontech; pre-equilibrated with buffer A and pre-coated with tRNA), and IgG was mixed with 3 µl of protein A sepharose (Amersham Biosciences; pre-equilibrated with buffer A and pre-coated with tRNA) at room temperature for 30 min. After washing out unbound protein, 40N RNA or the RNA pool after each round (40 µl) was subtracted by binding to TALON metal affinity resin (5 µl) and protein A sepharose bound to IgG (5 µl) and incubated for 30 min at room temperature. After washing out unbound protein, 40N RNA and the RNA pool after each successive round (40 µl) was incubated with TALON metal affinity resin and protein A sepharose bound to IgG for 30 min to subtract binding RNA species. Subtracted RNAs were collected by centrifugation at 1000 *g* for 30 s and the remaining RNA pools (40 µl) were added to TALON metal affinity resin pre-bound to RANK protein and incubated for 30 min at room temperature. RNA–protein complexes were isolated by centrifugation, washed twice with buffer A and eluted with buffer A containing 300 mM imidazole. RNAs were extracted by phenol/chloroform treatment and precipitated with ethanol. Then, cDNAs were synthesized with RAV-2 reverse transcriptase (Takara Co.), amplified by PCR using the N40 primer set and followed by T7 transcription. Selection II employed essentially the same procedures except that TALON metal affinity resin was pre-coated with polyA. Selection-amplification was repeated seven times for all selections. As the selection cycle proceeded, the stringency of selection was increased by decreasing the ratio of protein to RNA. The initial molar ratio 1:3 (3 µM protein to 9 µM RNA) was reduced to 1:25 (0.16 µM protein to 4 µM RNA) in the final round. cDNAs for selected RNAs were cloned into plasmid pGEM-T Easy Vector (Promega) and sequenced.

Table 1. *In vitro* selection scheme for RNA aptamers to RANK

Round	RANK (µM)	RNA (µM)	Ratio (protein/RNA)
1	3	9	1:3
2	2	8	1:4
3	1	7.5	1:7.5
4	0.7	7	1:10
5	0.4	6	1:15
6	0.25	5	1:20
7	0.16	4	1:25

The binding experiment was carried out at 25°C for 30 min and the assay volume was 50 µl. For reach round, pre-resin binding was subtracted.

Preparation of RNA aptamers for *in vitro* analysis

Selected sequences were amplified by PCR using 40N primer sets and the PCR products were used as templates for *in vitro* transcription. For surface plasmon resonance (SPR) analysis, synthetic oligonucleotides were used as templates for *in vitro* transcription. The parental sequence for the synthesis of apt1 short was 5′-TTTTTTTTTTTTTTTTTACGGTGTTCGTAGCCCTTCCCGATCCCACCCATACGAATCCGTCCTATAGTGAGTCGTATTA-3′. After synthesis of RNAs, DNA templates were digested with RNase-free DNase I (Takara Co.; 1 U/µg of template DNA). The resulting RNA was extracted by phenol/chloroform treatment and recovered by ethanol precipitation in the presence of 0.3 M sodium acetate (pH 6.5). The RNA pellet was rinsed with 70% ethanol, dried, dissolved in water and passed through a spin column (Micro Bio-spin column P-30, BioRad).

SPR analysis

The real-time measurement of the interaction between RANK and the selected RNA was performed using the BIAcore 2000 biosensor system (BIAcore AB) at 25°C according to the manufacturer's instruction and as described previously (17). Biotinylated-$(dT)_{16}$ (0.02 µg/µl) was bound to the surface of streptavidin-coated sensor chip SA (BIAcore AB) at a flow rate of 20 µl/min in the HBS-EP buffer (BIAcore AB: 0.01 M HEPES, pH7.4, 0.15 M NaCl, 0.005% Surfactant P20, 3 mM EDTA). After immobilization of biotinylated-$(dT)_{16}$, 3′-poly$(A)_{16}$-tagged RNA aptamers were immobilized by hybridization with a flow rate of 20 µl/min for 1 min. A blank flow cell was used to check for non-specific binding of RNAs. For monitoring the interaction using the BIAcore instrument, all procedures were automated to run repetitive cycles of sample injection (30 µl injection samples at a flow rate of 10 µl/min) and wash (10 µl wash buffer containing 8 M Urea). RANK and other proteins were diluted to various

concentrations in buffer A. Interaction was estimated by subtracting the response units of protein injected into a blank flow cell from the response of injected proteins into the RNA-immobilized flow cell.

Pull-down assay

The 3′-poly(A)$_{16}$-tagged RNA aptamer was incubated with Oligo(dT) Type7 cellulose (Amersham Biosciences; pre-equilibrated with buffer B: 10 mM Tris–HCl, pH 7.6, 2.5 mM magnesium acetate, 0.1 M KCl, 1 mM EDTA and 0.14 mg/ml BSA) for 30 min at room temperature. The mixture was centrifuged at 2100 *g* for 1 min and the resin was washed twice with buffer B. The aptamer-conjugated resin was dissolved in 50 µl of buffer B, incubated with 2 µg of human recombinant RANK in the presence or absence of RANKL (2 µg) for 15 min at room temperature, and the mixture was centrifuged at 2100 *g* for 1 min. The resin was washed three times with 150 µl of buffer B. Proteins bound to the aptamer were eluted with 15 µl of TE buffer (10 mM Tris Base, 1 mM EDTA, pH 8.0), supplemented with 1 µl of 10 mg/ml RNase A and subjected to SDS–PAGE (12%). RANK was immunostained with anti-human horseradish peroxidase (HRP)-conjugated IgG (Amersham Biosciences), which detects the Fc portion of the RANK-Fc chimera, according to the manufacturer's instructions. RANKL was detected by specific rabbit antibody against human soluble RANKL (Pepro Tech) using secondary anti-rabbit HRP-conjugated IgG (Amersham Biosciences). Signals were detected by means of enhanced chemiluminescence using ECL Western Blotting Detection System (Amersham Biosciences) according to the manufacturer's instructions.

RESULTS

Isolation of RNA aptamers to RANK

Affinity RNA selection experiments were performed using the recombinant human soluble RANK/IgG$_1$Fc chimera as the target and initial RNA pools of 40 random nucleotide positions (referred to as N40 RNA pool). *In vitro* selection was initiated using an N40 pool of 10^{14} different RNA molecules. In selection I, RNA molecules that bound to RANK/IgG$_1$Fc chimera (His-tagged) were captured by affinity precipitation using TALON metal affinity resin pre-coated with tRNA. In selection II, the same procedures were used except that RNA–RANK complexes were trapped on TALON metal affinity

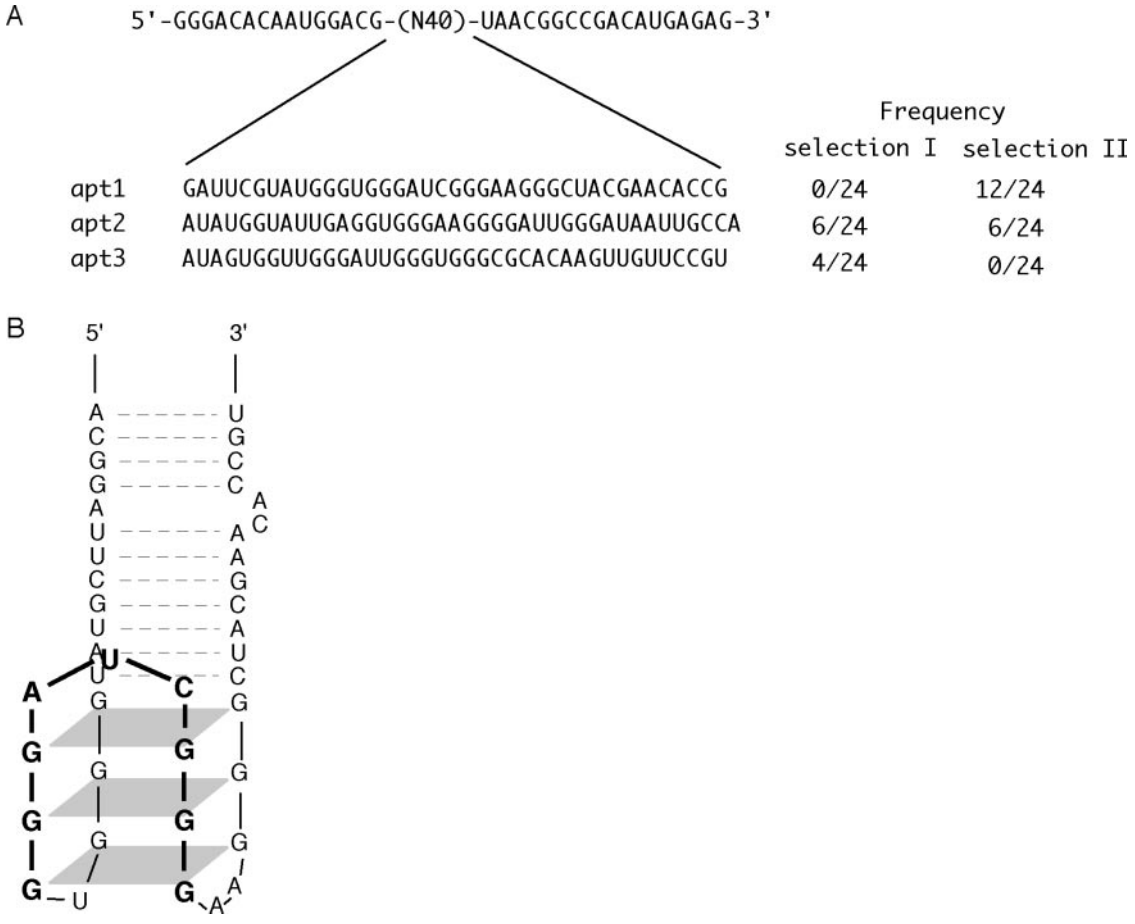

Figure 1. *In vitro* selected RNA sequences and potential G-quartet structure. (**A**) RNA sequences selected from randomized N40 RNA libraries. The sequence of the parental N40 RNA pool contains 5′ and 3′ constant sequences for primer annealing. After seven rounds of selection in two independent selection procedures (selection I and selection II), each of the 24 individual clones were selected and three non-homologous sequences were identified. The frequency of each sequence in these selections is shown as numbers of each clone found in 24 independent isolates. (**B**) Predicted G-quartet structure of the RANK aptamer (apt1).

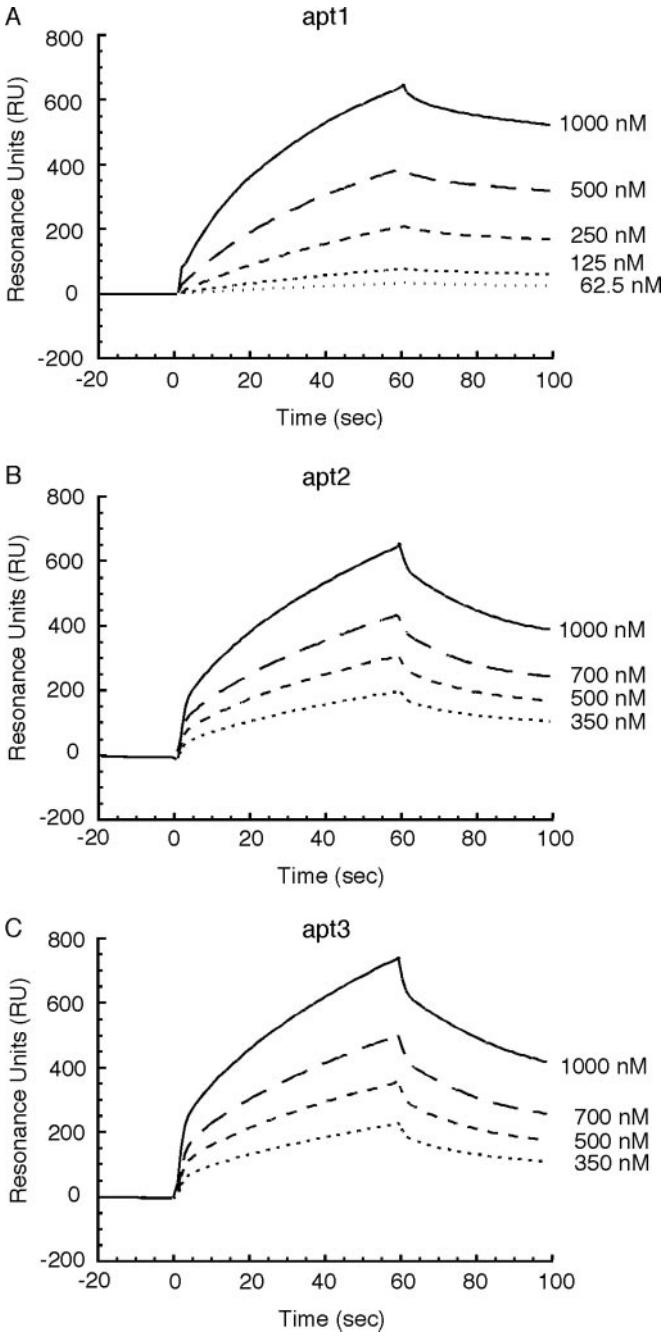

Figure 2. SPR sensorgrams of RANK binding to RNA aptamers. The indicated concentration of RANK was injected to a sensor chip immobilized with apt1 (**A**), apt2 (**B**) and apt3 (**C**) as well as to an empty (control) chip, and the net SPR signals were plotted. Experimental details and procedures are described in Materials and Methods.

resin pre-coated with poly(A). To eliminate matrix- or IgG-binding sequences, the RNA pool of each selection was pre-incubated with TALON resin and IgG, and unbound material was used for selection. The stringency of the selection was gradually increased by decreasing the relative ratio of input protein to RNA as the selection cycle proceeded. Twenty four RNA sequences from each selection were cloned and analyzed to monitor the progress of selection. After seven rounds of selection, all the selected RNAs could be grouped into either one of the three different sequences, referred to as apt1 through apt3 (Figure 1A).

The MFOLD prediction (18) for potential secondary structures failed to reveal a common structure for apt1 to apt3 RNAs (data not shown). It is known, however, that a G-quartet conformation that cannot be predicted by MFOLD is occasionally found in RNA aptamers (19–21). The presence of a minimum of four interspersed GG dinucleotides is the requirement for the G-quartet conformation, and the primary sequences of apt1 to apt3 RNAs contain four interspersed GGG trinucleotides (or GG dinucleotides) that meet this criterion (Figure 1A), suggesting that all the selected aptamers adopt G-quartet structures (Figure 1B).

Aptamer binding to RANK was monitored in real time with a BIAcore 2000 instrument based on SPR analysis. 3′-poly(A)-tailed RNAs were immobilized to the streptavidin sensor chip via 5′-biotinylated oligo(dT), and the formation of RANK-coupled complexes on this matrix was detected as SPR signals. No positive signal was observed in a blank flow cell (data not shown). (Note that the background Resonance Units (RUs) of RNAs and 5′-biotinylated oligo(dT) immobilized on chips were subtracted in all the sensorgrams.) SPR signals for apt1 to apt3 sensor chips appeared and increased in proportion to the amount (62.5–1000 nM) of RANK injected, while no positive signal was observed for the N40 random sensor chip (data not shown). The apparent dissociation constant (K_d) estimated from the SPR profile was 0.33, 1.8 and 5.8 μM for apt1, apt2 and apt3 RNAs, respectively (Figure 2A). Since these aptamers did not bind to either the Fc region in the intact IgG, an Fc-fusion to CD28 (data not shown) or to the histidine tag (data not shown), the selected aptamers bound directly to RANK in the chimera.

When the apt1 RNA was synthesized with 2′-Fluorine-dCTP and -dUTP instead of the canonical CTP and UTP, respectively, the apparent affinity of the modified RNA to RANK increased to the 0.1 μM K_d (data not shown). This was rather unexpected since all the aptamers selected in this laboratory were affected, more or less, by 2′-Fluorine modification in their binding affinity to target proteins.

Structure and sequence requirements for apt1 affinity to RANK

Since apt1 appeared most frequently in selection II and showed the highest affinity to RANK, it was chosen for further characterization. To determine the minimal sequence requirements for RANK binding, several truncated and mutated variants were generated from the 72 nt apt1 RNA. First, 5′ and 3′ deletions were made giving rise to three variants, i.e. apt1 short (Figure 3, middle), apt1 shortM4 (Figure 3, bottom left) and apt1 shortM5 (Figure 3, bottom right). The binding ability of these shortened RNAs to RANK was determined by BIAcore biosensor analysis. As shown in Figure 4, although aptamer affinity was reduced in proportion to the length of the deletions, apt1 shortM4 retained sufficient affinity to RANK, while apt1 shortM5 no longer bound to RANK. Apt1 shortM4 is 32 nt long and born from the random 40N sequences without any fixed flanking sequences.

To examine whether apt1 forms a G-quartet structure, we substituted the 5′ second GGG to AAA (apt1 fullM1), AAG (apt1 fullM2), GAA (apt1 fullM3) and GAG (apt1 fullM4)

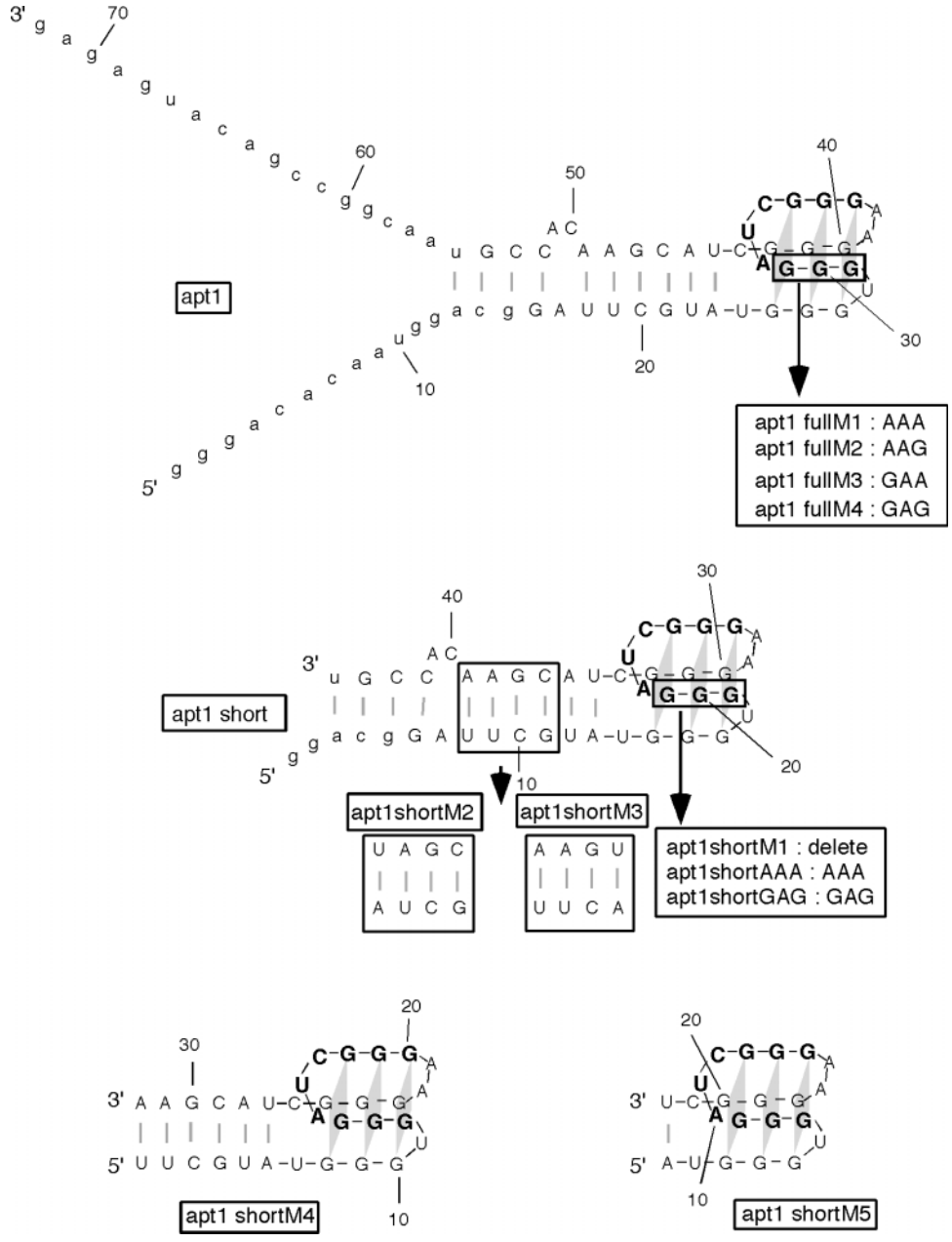

Figure 3. The secondary structure prediction of apt1 and its deletion or substitution variants. The original sequence of apt1 was altered by substituting AAA, AAG, GAA and GAG for the 5′ second G triplet, giving rise to apt1 fullM1 through fullM4 derivatives, respectively (top panel). An apt1 variant truncated at the 5′ and 3′ ends, apt1 short, was also altered by substitutions and internal deletions (middle). Further deletions were made at both termini to generate apt1 shortM4 and apt1 shortM5 (bottom). Nucleotide positions are counted from the 5′ terminus.

(see Figure 3, top). These substitutions led to complete loss of binding (data not shown). In addition, deletion of GGG (apt1 short M1) as well as the substitution of GAG (apt1 shortGAG) or AAA (apt1 shortAAA) for GGG also abrogated the aptamer's affinity to RANK (Figure 4A and B). The apt1 contains a UUCG tetranucleotide sequence that is predicted to be in the stem portion, but it may also form a thermodynamically stable UNCG loop that would not be conducive to forming a G-quartet structure (19,22,23). To confirm the likely structure of this region, the base pairs U8:A39 and G11:C36 were substituted by the base pairs A8:U39 (apt1 shortM2) and A11:U36 (apt1 shortM3), respectively, to disrupt the possible UNCG sequence motif (see Figure 3, middle). These substitutions conferred on apt1 short an increased affinity to RANK (Figure 4B), confirming the formation of the G-quartet structure and its crucial role in binding to RANK.

Apt1 does not interfere with RANK–RANKL interaction but forms a ternary complex

The RANK ligand, RANKL, self-associates as a homotrimer and complexes with RANK in a molar ratio of 3:1 (24), leading to osteoclast differentiation. We first examined whether apt1 inhibits the RANK–RANKL interaction. Apt1 RNA-conjugated

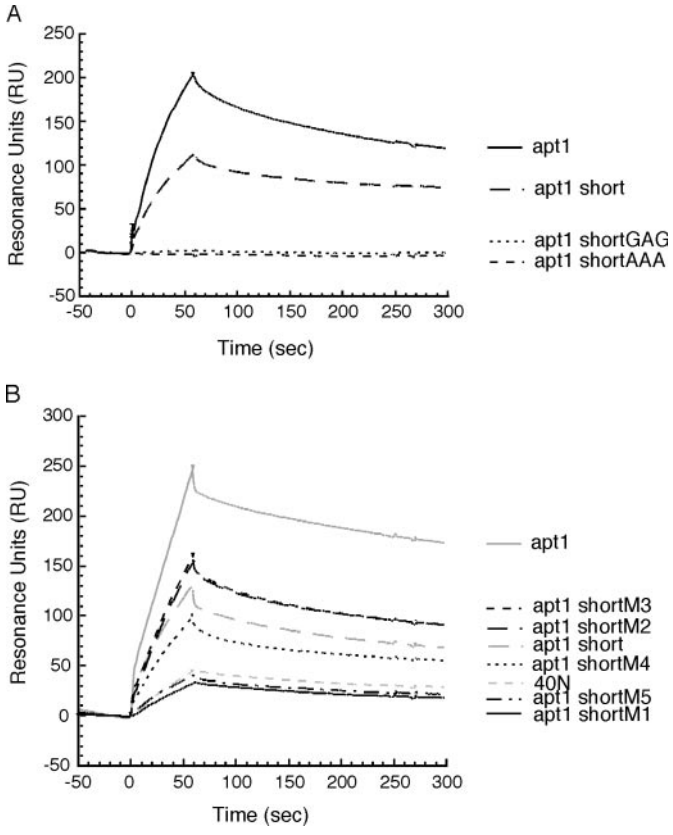

Figure 4. Affinity of apt1 deletion and substitution variants to RANK. RANK protein (0.5 μM) was injected to the flow cells immobilized with the indicated RNA aptamers as well as to a control cell, and the net SPR signals are plotted. (**A**) Apt1 variants changed at the G-quartet structure. (**B**) Apt1 variants changed at the 5′ and 3′ termini as well the predicted stem. Experimental details and procedures are described in Materials and Methods.

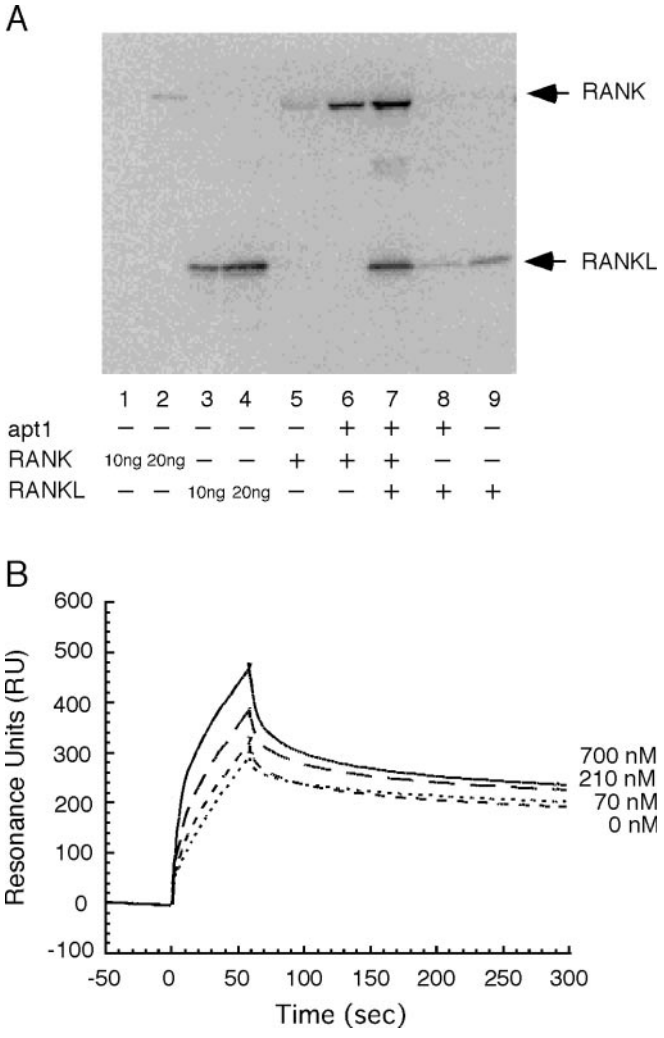

Figure 5. The formation of the apt1–RANK–RANKL ternary complex. (**A**) Pull-down assay. Oligo(dT) cellulose resin conjugated with apt1 (10 μg) was injected with RANK (i.e. RANK-Fc chimera) and/or RANKL (2 μg). Proteins bound to the RNA-resin were spun down and subjected to SDS–PAGE. RANK and RANKL were detected by western blot analysis using specific antibodies as described in Materials and Methods. Samples: lanes 1 through 4, RANK and RANKL protein standard (10 or 20 ng) prior to the co-precipitation experiments; lane 5, immobilized resin (no RNA) + RANK in the absence of RANKL; lane 6, apt1-immobilized resin + RANK in the absence of RANKL; lane 7, apt1-immobilized resin + RANK in the presence of RANKL; lane 8, apt1-immobilized resin + RANKL in the absence of RANK; lane 9, immobilized resin (no RNA) + RANKL in the absence of RANK. (**B**) The formation of the apt1–RANK–RANKL ternary complex on the BIAcore sensor chip. Apt1-immobilized sensor chip was co-injected with RANK protein (700 nM) and RANKL (0–700 nM), and the net SPR signals were plotted as described in Materials and Methods.

resin was mixed with RANK in the presence or absence of RANKL. The resulting complexes were spun down and bound proteins were analyzed by immunoblotting using specific antibodies against RANK and RANKL. Although a small level of non-specific binding of RANK or RANKL to resin was observed in the absence of apt1 RNA (Figure 5A, lanes 5 and 9; this non-specific binding was not blocked by adding BSA to the resin), RANK efficiently bound to the apt1-conjugated resin (Figure 5A, lane 6). Under these conditions, RANKL did not bind to the apt1-conjugated resin in the absence of RANK (except for the non-specific binding to resin; Figure 5A, lanes 8 and 9) but bound efficiently in the presence of RANK (Figure 5A, lane 7). This result suggests that apt1 does not interfere with the RANK–RANKL interaction and rather a ternary complex, apt1–RANK–RANKL, is formed.

The formation of the apt1–RANK–RANKL ternary complex was directly monitored by BIAcore analysis. The 3′-poly (A)-tailed apt1 RNA was immobilized to the streptavidin sensor chip via 5′-biotinylated oligo(dT). RANK (700 nM) and different amounts of RANKL (0–700 nM) were co-injected at a flow rate of 10 μl/min for 60 s and dissociated for 240 s by injecting a blank solution at the same flow rate. As expected, SPR signals on the apt1 sensor chip increased in proportion to the 70, 210 and 700 nM RANKL co-injections (Figure 5B), while no positive signal was observed for the same apt1 sensor chip in the absence of RANK (data not shown). The increase in the SPR signal can be interpreted to indicate the formation of the apt1–RANK–RANKL ternary complex on the sensor chip. The other aptamers, apt2 and apt3, also showed the same result (data not shown).

Selectivity of apt1 for capturing the TNFR family proteins

The TNF ligand and receptor families are conserved, and therefore, several TNF ligand family proteins utilize multiple

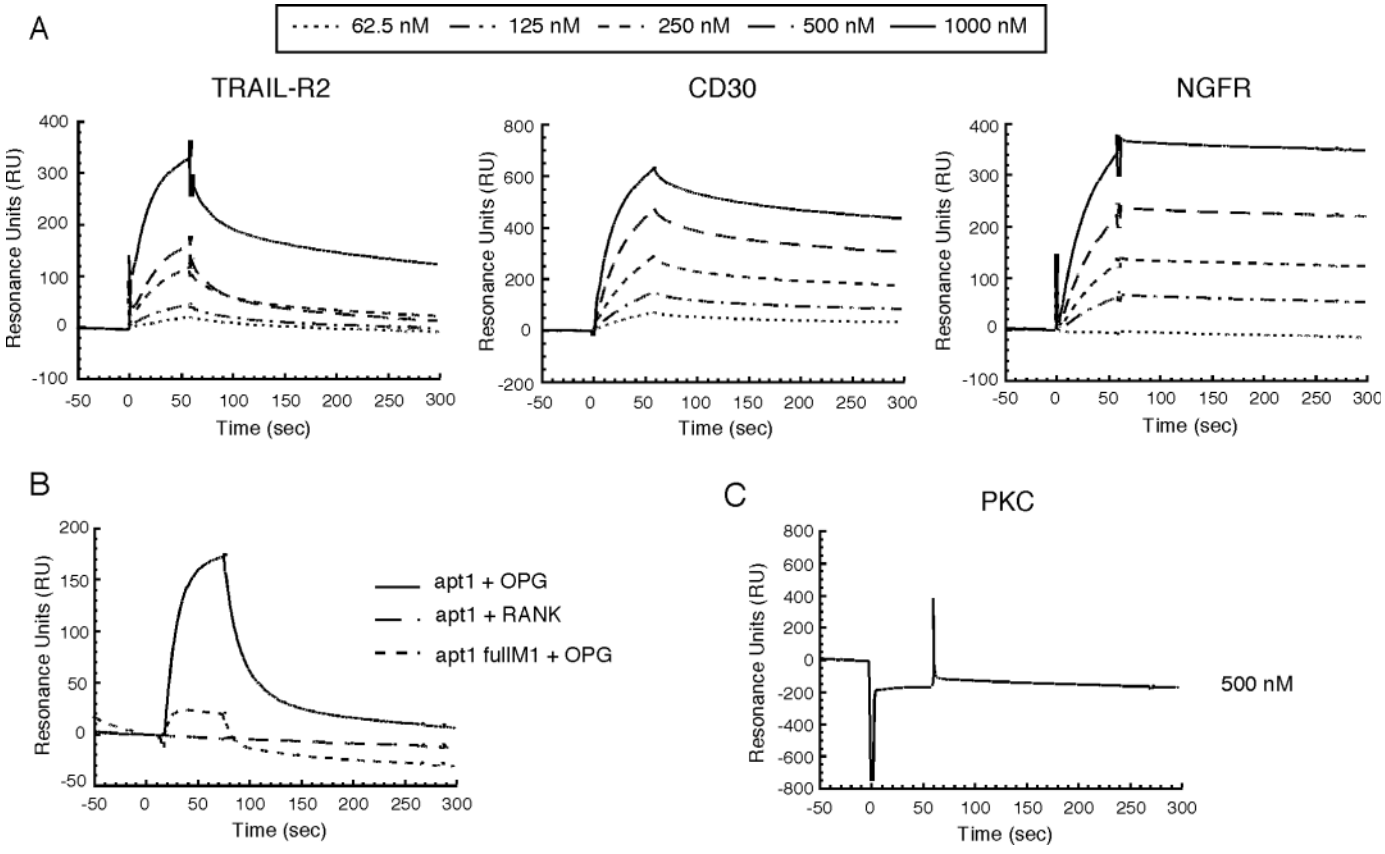

Figure 6. The binding specificity of apt1, selected to RANK, to other TNF receptor family proteins. The apt1-immobilized sensor chip was injected with the indicated concentrations of TNF receptor proteins and PKC (control) and the potassium acetate concentrations listed below. (**A**) TRAIL-R2 in binding buffer containing 80 mM potassium acetate (left), CD30 in binding buffer containing 200 mM potassium acetate (middle) and NGFR in binding buffer containing 200 mM potassium acetate (right). (**B**) OPG (125 nM) in binding buffer containing 400 mM potassium acetate. Note that OPG bound efficiently to the apt1-sensor chip, but much less to the non-functional apt1 mutant apt1 fullM1. Under these conditions, RANK no longer bound to apt1. (**C**) PKC (500 nM) in binding buffer containing 400 mM potassium acetate.

TNF receptors (2–6). We, therefore, investigated whether apt1 is specific to (human) RANK or reactive to other tumor necrosis factor receptor (TNFR) family proteins using BIAcore analysis. The apt1-immobilized sensor chip was injected with mouse RANK, TRAIL-R2, CD30, NGFR and OPG as well as a set of negative control proteins, such as PKC and CD28. During the course of this study, we found that some of these test proteins bound to a dysfunctional-apt1 variant (apt1 fullM1, G-quartet nullified) sensor chip when standard buffer A was used for protein injection (data not shown). This (G-quartet independent) background binding, however, was eliminated in the presence of 200 mM potassium acetate for CD30 and NGFR. A set of sensorgrams for these TNFR protein associations with apt1 RNA is shown in Figure 6A, and their estimated kinetic parameters are summarized in Table 2. It was evident that TRAIL-R2, CD30 and NGFR bound to the apt1 RNA, and the SPR signals increased in proportion to the amount injected. Once again, in the conditions of this analysis, no SPR signals were detectable on the apt1 fullM1 sensor chip (data not shown). Of the estimated K_d values, CD30 showed unexpectedly high affinity to apt1 (discussed below). OPG, a decoy receptor for RANK, also bound to apt1, although a small but significant level of non-specific binding to the apt1 fullM1 RNA could not be eliminated even in the presence of 400 mM potassium acetate (Figure 6B). It was remarkable that apt1 is able to capture OPG even in the presence of 400 mM potassium acetate, where apt1 no longer captures RANK (see Figure 6B). Under any assay conditions tested, PKC did not show specific binding to apt1 even though PKC contains cysteine-rich domains (CRDs) similar to the TNFR family proteins (Figure 6C). Another control protein, CD28-Fc chimera, did not bind to apt1 (data not shown). These results indicate that apt1 recognizes a common structure of the TNFR family proteins and therefore apt1 may have potential as a broad-spectrum therapeutic agent for additional TNFR-related diseases.

Table 2. Kinetic parameters of the interaction between TNF receptor family proteins and apt1 estimated by BIAcore analysis

TNFR family proteins	KOAc (mM)	Dissociation constant (nM)	Association rate (M^{-1} s^{-1})	Dissociation rate (s^{-1})
Human RANK	80	300	1.5×10^4	4.4×10^{-3}
Mouse RANK	80	110	5.5×10^4	5.8×10^{-3}
TRAIL-R2	80	960	1.4×10^4	1.3×10^{-2}
CD30	200	0.11	3.4×10^4	3.8×10^{-6}
NGFR	200	870	1.9×10^4	1.7×10^{-3}
Human RANK	200	130	5.6×10^2	7.0×10^{-5}

Values were estimated from the sensorgrams shown in Figure 6. At these potassium acetate concentrations, a dysfunctional-apt1 variant (apt1 fullM1, G-quartet nullified) did not bind to these test proteins.

DISCUSSION

In this study, we isolated RNA aptamers to the extracellular domain of RANK. One of them, apt1, which showed the highest affinity to RANK, was studied in detail. RNA sequence deletion and substitution experiments combined with BIAcore-binding analysis revealed that a minimum of 32 nt sequence (apt1 shortM4 variant) constitutes the affinity of apt1 to RANK. This sequence encodes a G-quartet structure that is vital for binding to RANK. G-quartets represent an important structural element in a number of natural nucleic acid sequences including telomeric DNA structures (25), HIV-1 RNA dimers (26) and mRNAs that are regulated by G-quartet binding protein FMRP [(fragile X mental retardation protein; (27)]. In the literature, several *in vitro* selected nucleic acids that contain G-quartet motifs have been reported: e.g. DNA aptamers selected against DNA enzymes (19), RNA aptamers against the prion protein PrP (20) and RNA aptamers against flavin and nicotinamide redox cofactors (21). One of them, the thrombin DNA aptamer, is 15 nt long and adopts a highly compact G-quartet structure sufficient for binding to thrombin (28,29). In contrast to the thrombin aptamer, the apt1 shortM5 RNA was unable to bind to RANK, although it is 22 nt long and able to form a G-quartet structure. Therefore, although the G-quartet structure is vital for the interaction with RANK, other sequence or structural elements are important as well.

The selected RNA aptamers, apt1 through apt3, bound to RANK and did not compete with the RANK ligand, RANKL, for binding. Rather, an apt1–RANK–RANKL ternary complex was formed on the apt1-immobilized sensor chip or resin. Therefore, apt1 does not bind to a ligand-binding site in RANK but to other site(s) where the aptamer binding does not induce any inhibitory conformational change. Incidentally, even though selection was against RANK, apt1 was able to bind to other TNFR family proteins, such as TRAIL-R2, CD30, NGFR and OPG. Therefore, the apt1-binding site in RANK is a common structure that does not overlap the ligand-binding site in the TNFR family proteins.

One such candidate target of RANK might be the CRD conserved in the TNF receptors. The extracellular domains of TNF receptors are characterized by the presence of CRDs, which are pseudo repeats typically containing six cysteines engaged in the formation of three disulfide bonds (30). The common structure in the TNFR family proteins examined in this study (i.e. TRAIL-R2, CD30, NGFR and OPG) is an A1-B2 module, which is a typical CRD (30). A1 modules are 12–27 amino acids long, consisting of three short β-strands and one disulfide bridge. B2 modules are 21–24 amino acids long, comprising three anti-parallel strands and two disulfide bridges. However, it is known that CRD serves as a site for binding to TNFR ligands (30). Therefore, if apt1 binds to CRDs, the apt1-binding site must be topologically distinct from the ligand-binding site in CRDs of TNF receptors.

TNF ligands share a common structural motif termed the TNF homology domain (THD) (30). The THD is a 150 amino acid long sequence containing a conserved framework of aromatic and hydrophobic residues. A structural study has revealed that THDs share a virtually identical tertiary fold and associate to form trimeric proteins (31–38). The THDs adopt a classical 'jelly role' topology, and trimeric THDs are ~60 Å in height, resembling bell-shaped, truncated pyramids. The structural basis of the TNF receptor and ligand interaction has been unraveled by the first crystallographic structure of a TNF ligand (LTα) bound to its cognate receptor (TF-R1) (33). The asymmetric unit contains three receptors and three ligands assembled as a hexameric complex in which a TNF trimer binds to three receptor molecules. More recently, highly similar crystal structures have been reported for complexes between TRAIL and TRAIL-R2, confirming that a 3:3 (three trimers versus three receptors) stoichiometry is the likely basis of the signaling unit (35,36,38). These structural data point out that the bell-shaped, truncated pyramid of trimeric THDs docks inside a pocket formed by the interaction of three receptor CRD molecules. Since apt1 does not compete with RANKL for binding to RANK, we speculate that apt1 binds to the exterior surface of the CRDs and this would be compatible for the ligand binding to the interior surface of the CRDs, as shown for THD. Of TNF receptors tested, CD30 showed extremely high affinity to apt1 (see Table 2). The number of CRDs in a given receptor varies from one to four, except in the case of CD30 where the three CRDs have been partially duplicated in the human but not in the mouse sequence. The repeated and regular arrangement of CRDs confers an elongated shape upon the receptors (30). This structural feature could account for the increased affinity of CD30 to apt1. An ongoing NMR study will solve this problem (T. Sakamoto, T. M., G. Kawai, Y. N., manuscript in preparation).

The potent biological roles of TNF/TNFR families in human diseases indicate that they would make a good target to ameliorate certain illnesses (39). Pharmaceuticals to inhibit TNF have been developed, which control previously recalcitrant inflammatory conditions, such as RA and inflammatory bowel disease (40,41). Indeed, TNF and other TNF/TNFR family proteins are now being targeted for therapies against widespread human diseases, such as atherosclerosis, osteoporosis, autoimmune disorders, allograft rejection and cancer. From this viewpoint, RNA aptamers to RANK might have potential for therapies against osteoclastogenesis. The selected RNA aptamers in this study, however, were not inhibitory to the ligand interaction with the receptor molecule RANK (see Figure 5). Nevertheless, it cannot be excluded that the formation of the apt1–RANK–RANKL ternary complex may affect downstream signaling. We aimed at testing this possibility in cultured cell osteoclast differentiation. However, standard culture medium (such as α-MEM and others) was not appropriate for the formation of G-quartet structures, which requires an optimum concentration of K^+ ion (42). High sodium concentration in α-MEM (5.3 mM K^+ and 120 mM Na^+) was inhibitory to the G-quartet structure, and the addition of potassium in different concentrations failed to restore the G-quartet formation (data not shown). Therefore, we have no answer to whether the formation of the apt1–RANK–RANKL ternary complex affects downstream signaling or not. Nevertheless, these aptamers might prove useful as a tool to detect or affinity purify TNFR family proteins in the appropriate solution conditions since 2′-Fluorine-modified apt1 RNA achieved higher affinity and extreme stability as well. Taking these into consideration, the present data provide us with an experimental basis toward the future design and selection for effective RNA aptamers to the TNF receptor family proteins and ligands.

ACKNOWLEDGEMENTS

We thank Jin Gohda and Jun-ichiro Inoue for their expertise and support for the osteoclast differentiation assay. Colin Crist is thanked for critical reading of the manuscript and valuable suggestions. This work was supported in part by grants from the following: The Ministry of Education, Sports, Culture, Science and Technology of Japan (MEXT); the Organization for Pharmaceutical Safety and Research (OPSR); and The Japan Health Sciences Foundation.

REFERENCES

1. Nakagawa,N., Kinosaki,M., Yamaguchi,K., Shima,N., Yasuda,H., Yano,K., Morinaga,T. and Higashio,K. (1998) RANK is the essential signaling receptor for osteoclast differentiation factor in osteoclastogenesis. *Biochem. Biophys. Res. Commun.*, **253**, 395–400.
2. Beutler,B. and van Huffel,C. (1994) Unraveling function in the TNF ligand and receptor families. *Science*, **264**, 667–668.
3. Smith,C.A., Frrah,T. and Goodwin,R.G. (1994) The TNF receptor superfamily of cellular and viral proteins: activation, costimulation, and death. *Cell*, **76**, 959–962.
4. Cosman,D. (1994) A family of ligands for the TNF receptor superfamily. *Stem Cells*, **12**, 440–455.
5. Gruss,H.J. and Dower,S.K. (1995) Tumor necrosis factor ligand superfamily: involvement in the pathology of malignant lymphomas. *Blood*, **85**, 3378–3404.
6. Ashkenazi,A. and Dixit,V.M. (1998) Death receptors: signaling and modulation. *Science*, **281**, 1305–1308.
7. Gravallese,E.M., Galson,D.L., Goldring,S.R. and Auron,P.E. (2001) The role of TNF-receptor family members and other TRAF-dependent receptors in bone resorption. *Arthritis Res.*, **3**, 6–12.
8. Hofbauer,L.C., Neubauer,A. and Heufelder,A.E. (2001) Receptor activator of nuclear factor-kappaB ligand and osteoprotegerin: potential implications for the pathogenesis and treatment of malignant bone diseases. *Cancer*, **92**, 460–470.
9. Body,J.J., Greipp,P., Coleman,R.E., Facon,T., Geurs,F., Fermand,J.P., Harousseau,J.L., Lipton,A., Mariette,X., Williams,C.D., Nakanishi,A., Holloway,D., Martin,S.W., Dunstan,C.R. and Bekker,P.J. (2003) A phase I study of AMGN-0007, a recombinant osteoprotegerin construct, in patients with multiple myeloma or breast carcinoma related bone metastases. *Cancer*, **97**, 887–892.
10. Wilson,D.S. and Szostak,J.W. (1999) *In vitro* selection of functional nucleic acids. *Annu. Rev. Biochem.*, **68**, 611–647.
11. Brody,E.N. and Gold,L. (2000) Aptamers as therapeutic and diagnostic agents. *J. Biotechnol.*, **74**, 5–13.
12. Rabin,R., Lochrie,M., Janjic,N. and Gold,L. (2002) Nucleic acid ligands which bind to hepatocyte growth factor/scatter factor (HGF/SF) or its receptor c-met. Patente [US-6344321 B1] Number Issue, 6344321.
13. Daniels,D.A., Sohal,A.K., Rees,S. and Grisshammer,R. (2002) Generation of RNA aptamers to the G-protein-coupled receptor for neurotensin, NTS-1. *Anal. Biochem.*, **305**, 214–226.
14. Anderson,D.M., Maraskovsky,E., Billingsley,W.L., Dougall,W.C., Tometsko,M.E., Roux,E.R., Teepe,M.C., DuBose,R.F., Cosman,D. and Galibert,L. (1997) A homologue of the TNF receptor and its ligand enhance T-cell growth and dendritic-cell function. *Nature*, **390**, 175–179.
15. Tuerk,C. and Gold,L. (1990) Systematic evolution of ligands by exponential enrichment: RNA ligands to bacteriophage T4 DNA polymerase. *Science*, **249**, 505–510.
16. Oguro,A., Ohtsu,T., Svitkin,Y., Sonenberg,N. and Nakamura,Y. (2003) RNA aptamers to initiation factor 4A helicase hinder cap-dependent translation by blocking ATP hydrolysis. *RNA*, **9**, 394–407.
17. Ishino,T., Atarashi,K., Uchiyama,S., Yamami,T., Saihara,Y., Yoshida,T., Hara,H., Yokose,K., Kobayashi,Y. and Nakamura,Y. (2000) Interaction of ribosome recycling factor and elongation factor EF-G with *E.coli* ribosomes studied by the surface plasmon resonance technique. *Genes Cells*, **5**, 953–963.
18. SantaLucia,J.,Jr (1998) A unified view of polymer, dumbbell and oligonucleotide DNA nearest-neighbor thermodynamics. *Proc. Natl Acad. Sci. USA*, **95**, 1460–1465.
19. Breaker,R.R. (1997) DNA aptamers and DNA enzymes. *Curr. Opin. Chem. Biol.*, **1**, 26–31.
20. Weiss,S., Proske,D., Neumann,M., Groschup,M.H., Kretzschmar,H.A., Famulok,M. and Winnacker,E.L. (1997) RNA aptamers specifically interact with the prion protein PrP. *J. Virol.*, **71**, 8790–8797.
21. Lauhon,C.T. and Szostak,J.W. (1995) RNA aptamers that bind flavin and nicotinamide redox cofactors. *J. Am. Chem. Soc.*, **117**, 1246–1257.
22. Uhlenbeck,O.C. (1990) Tetraloops and RNA folding. *Nature*, **346**, 613–614.
23. Smirnov,I. and Shafer,R.H. (2000) Lead is unusually effective in sequence-specific folding of DNA. *J. Mol. Biol.*, **296**, 1–5.
24. Lam,J., Nelson,C.A., Ross,F.P., Teitelbaum,S.L. and Fremont,D.H. (2001) Crystal structure of the TRANCE/RANKL cytokine reveals determinants of receptor-ligand specificity. *J. Clin. Invest.*, **108**, 971–979.
25. Blackburn,E.H. (1991) Structure and function of telomeres. *Nature*, **350**, 569.
26. Sundquist,W.I. and Heaphy,S. (1993) Evidence for interstrand quadruplex formation in the dimerization of human immunodeficiency virus 1 genomic RNA. *Proc. Natl Acad. Sci. USA*, **90**, 3393–3397.
27. Kaytor,M.D. and Orr,H.T. (2001) RNA targets of the fragile X protein. *Cell*, **107**, 555–557.
28. Bock,L.C., Griffin,L.C., Latham,J.A., Vermaas,E.H. and Toole,J.J. (1992) Selection of single-stranded DNA molecules that bind and inhibit human thrombin. *Nature*, **355**, 564–566.
29. Macaya,R.F., Schultze,P., Smith,F.W., Roe,J.A. and Feigon,J. (1993) Thrombin-binding DNA aptamer forms a unimolecular quadruplex structure in solution. *Proc. Natl Acad. Sci. USA*, **90**, 3745–3749.
30. Bodmer,J.L., Schneider,P. and Tschopp,J. (2002) The molecular architecture of the TNF superfamily. *Trends Biochem. Sci.*, **27**, 19–26.
31. Eck,M.J. and Sprang,S.R. (1989) The structure of tumor necrosis factor-α at 2.6 Å resolution. Implications for receptor binding. *J. Biol. Chem.*, **264**, 17595–17605.
32. Jones,E.Y., Stuart,D.I. and Walker,N.P. (1989) Structure of tumour necrosis factor. *Nature*, **338**, 225–228.
33. Banner,D.W., D'Arcy,A., Janes,W., Gentz,R., Schoenfeld,H.J., Broger,C., Loetscher,H. and Lesslauer,W. (1993) Crystal structure of the soluble human 55 kd TNF receptor–human TNF β complex: implications for TNF receptor activation. *Cell*, **73**, 431–445.
34. Karpusas,M., Hsu,Y.M., Wang,J.H., Thompson,J., Lederman,S., Chess,L. and Thomas,D. (1995) 2 Å crystal structure of an extracellular fragment of human CD40 ligand. *Structure*, **3**, 1031–1039.
35. Cha,S.S., Sung,B.J., Kim,Y.A., Song,Y.L., Kim,H.J., Kim,S., Lee,M.S. and Oh,B.H. (2000) Crystal structure of TRAIL–DR5 complex identifies a critical role of the unique frame insertion in conferring recognition specificity. *J. Biol. Chem.*, **275**, 31171–31177.
36. Hymowitz,S.G., Christinger,H.W., Fuh,G., Ultsch,M., O'Connell,M., Kelley,R.F., Ashkenazi,A. and de Vos,A.M. (1999) Triggering cell death: the crystal structure of Apo2L/TRAIL in a complex with death receptor 5. *Mol. Cell*, **4**, 563–571.
37. Hymowitz,S.G., O'Connell,M.P., Ultsch,M.H., Hurst,A., Totpal,K., Ashkenazi,A., de Vos,A.M. and Kelley,R.F. (2000) A unique zinc-binding site revealed by a high-resolution X-ray structure of homotrimeric Apo2L/TRAIL. *Biochemistry*, **39**, 633–640.
38. Mongkolsapaya,J., Grimes,J.M., Chen,N., Xu,X.N., Stuart,D.I., Jones,E.Y. and Screaton,G.R. (1999) Structure of the TRAIL–DR5 complex reveals mechanisms conferring specificity in apoptotic initiation. *Nature Struct. Biol.*, **6**, 1048–1053.
39. Chan,K.F., Siegel,M.R. and Lenardo,J.M., (2000) Signaling by the TNF receptor superfamily and T cell homeostasis. *Immunity*, **13**, 419–422.
40. Taylor,P.C., Williams,R.O. and Maini,R.N., (2000) Anti-TNF alpha therapy in rheumatoid arthritis—current and future directions. *Curr. Dir. Autoimmun.*, **2**, 83–102.
41. Papadakis,K.A. and Targan,S.R. (2000) The role of chemokines and chemokine receptors in mucosal inflammation. *Inflamm. Bowel Dis.*, **6**, 303–313.
42. Guschlbauer,W., Chantot,J.F. and Thiele,D. (1990) Four-stranded nucleic acid structures 25 years later: from guanosine gels to telomer DNA. *J. Biomol. Struct. Dyn.*, **8**, 491–511.